Available online at www.sciencedirect.com

ScienceDirect

Acta Materialia 64 (2014) 100–112

Acta MATERIALIA

www.elsevier.com/locate/actamat

Interface structure of Nb films on single crystal MgO(100) and MgO(111) substrates

E.G. Fu [a,b,*], Y. Fang [c], M.J. Zhuo [d], S.J. Zheng [d], Z.X. Bi [d], Y.Q. Wang [b], M. Tang [b], X. Ding [c,*], W.Z. Han [d], H.M. Luo [e], J.K. Baldwin [d], A. Misra [d], M. Nastasi [f]

[a] State Key Laboratory of Nuclear Physics and Technology, School of Physics, Peking University, Beijing 100871, People's Republic of China
[b] Materials Science and Technology Division, Los Alamos National Laboratory, Los Alamos, NM 87544, USA
[c] State Key Laboratory for Mechanical Behavior of Materials, Xi'an Jiaotong University, Xi'an, People's Republic of China
[d] Materials Physics and Application Division, Los Alamos National Laboratory, Los Alamos, NM 87544, USA
[e] Department of Chemical Engineering, New Mexico State University, Las Cruces, NM 88003, USA
[f] Nebraska Center for Energy Sciences Research, University of Nebraska – Lincoln, Lincoln, NE 68508, USA

Received 21 September 2012; received in revised form 3 November 2013; accepted 10 November 2013
Available online 20 December 2013

Abstract

This study systematically investigates the interface structure of Nb films grown on MgO substrates with different orientations ((100) and (111)) by experiments and simulations. X-ray diffraction, transmission electron microscopy (TEM) and high-resolution TEM (HRTEM) were used to characterize the structure of Nb films and the structure of interfaces between Nb films and MgO substrates. The results show that thin films exhibit different preferred planes on different orientations of MgO substrates. First-principles calculations were used to understand the interface configuration through a coherent interface model. The combination of experiments and simulations shows that the work of separation, together with substrate orientation and lattice mismatch, determines the interface structure between films and substrates.

Keywords: Interface structure; TEM and HRTEM; First principles; Lattice mismatch; Work of separation

1. Introduction

Studies on interfaces in composite materials have attracted much attention in modern materials science since these materials have practical applications in many fields, such as coatings, sensors, photovoltaic devices, microelectronics devices, superconductors and catalysts [1–6]. Recently, new applications of interfaces concerning the enhancement of radiation tolerance of materials by manipulating interfaces, which act as powerful sinks for point defects and assist the recombination process between interstitials and vacancies, have been reported [7–14]. The interfaces in thin film materials play key roles in controlling their epitaxial quality, mechanical, physical, chemical, structural and functional properties [15–17]. As one of the major types of interfaces, metal/oxide interfaces exhibit specific properties, including magnetic, catalytic and tribological properties, and have been widely studied both in experiments and in simulations [1,18]. A fundamental understanding of interface structure at the atomic scale is considered to be necessary for the further development of film properties. Atomic observations of many metal/oxide interfaces, such as Au/MgO, Ag/CdO, Nb/Al_2O_3, Cu/Al_2O_3, Pt/NiO and Cu/NiO, have been reported [1,19–22]. As a major component of a number of metal/oxide interfaces, single crystal MgO is widely used as a substrate

* Corresponding authors. Address: State Key Laboratory of Nuclear Physics and Technology, School of Physics, Peking University, Beijing 100871, People's Republic of China (E.G. Fu).
E-mail addresses: efu@pku.edu.cn, fuengang@gmail.com (E.G. Fu), dingxd@mail.xjtu.edu.cn (X. Ding).

1359-6454/$36.00
http://dx.doi.org/10.1016/j.actamat.2013.11.031

material because it has a simple sodium chloride structure and clean MgO surfaces are easy to obtain. Epitaxial growth of metals on single crystal MgO has frequently been reported. Lu and Cosandey studied the interface structure in metal/MgO(100) interfaces by electron microscopy [23,24]. They concluded that Cu/MgO and Pd/MgO(100) interfaces are partially coherent and the contrast variation in high-resolution transmission electron microscopy (HRTEM) images is due to interfacial dislocations. They defined the dislocation structure of (001) and (111) interfaces based on coincidence-site lattice (CSL) and displacement shift complete (DSC) lattice models [23–26]. Trampert et al. reported HRTEM studies of the Ag/MgO interface made by molecular beam epitaxy (MBE) growth and revealed the interface structure by experiments and simulations [27]. The Ag/MgO(100) couple exhibits a preferential orientation of the Ag(100) plane parallel to the (100) surface of the MgO substrate. HRTEM shows a square network of edge-type dislocations with [100] line directions and Burgers vectors of the type $b = 1/2$Ag[100] [27]. Comparative theoretical studies of Ag/MgO(100) and Ag/MgO(110) interfaces concluded that chemical bond formation is not important for either Ag/MgO(100) or Ag/MgO(110) perfect interfaces, and the physical adhesion associated with polarization and charge redistribution are the dominant effects [28]. Chen et al. studied the interfaces of Cu/MgO(111) and Pd/MgO(111) by HRTEM and concluded that their interfaces have a cube-on-cube orientation relationship. A periodic localized interfacial dislocation contrast in both Cu/MgO(111) and Pd/MgO(111) interfaces was observed along the MgO[110] direction [29].

While the interface structures of metal/MgO thin film couples have been extensively studied, most of the studies have focused on face-centered cubic (fcc)/MgO interfaces, with few studies being performed on the interfaces of body-centered cubic (bcc)/MgO. Ikuhara et al. studied the atomic structure of MgO/V/MgO multilayer films grown by MBE, and they reported on the orientation relationship and interfacial dislocations between bcc V and MgO(100) in multilayer films [30]. Another study focused on the atomic and electronic structure of V/MgO interfaces with the V film thickness of 5 nm [31]. The comparison between the experimental and theoretical details by molecular orbital calculation found the presence of a hybridized orbital of V3*d* with Mg3*p* [31]. However, the detailed atomic structure of the interface and the fundamental mechanisms for forming orientation relationships of the interface in bcc/MgO thin films have not been widely studied and are not well understood. Furthermore, to the best of our knowledge, very few studies on the atomic interface structure of bcc metals on single crystal MgO(111) have been reported. In the present paper, the interface structures of Nb films grown on MgO(100) and MgO(111) substrates are systematically investigated by the combination of experiments and simulations. The studies reveal fundamental mechanisms that control the orientation relationships of interfaces in both thin films.

2. Experimental

Nb thin films were deposited on single crystal MgO(100) and MgO(111) substrates by means of electron-beam evaporation. The substrate temperature was set at 950 °C, and the deposition rate was 5 Å s^{-1}. The thickness of Nb thin films was 180 nm. The purity of the Nb evaporation target was 99.999%. The pure single crystal MgO(100) and MgO(111) substrates have dimension of 10 mm × 10 mm × 0.5 mm. The misorientation of (100) in MgO(100) substrate and (111) in MgO(111) substrate is less than 0.5°. The surface of substrates was polished by chemical mechanical polishing (CMP) technology with minimum sub-surface damage and possessed a surface roughness less than 1 nm. The substrates were immediately loaded into a vacuum chamber for thin film deposition to avoid surface roughening and hydroxide formation after they were removed from a clean plastic bag packed under 1000 class clean room conditions.

X-ray diffraction (XRD) analysis was used to characterize the Nb thin film structure and the orientation relationship between the film and the substrate. TEM experiments were performed on an FEI Tecnai F30 transmission electron microscope operated at 300 kV with a field-emission gun, and images were recorded by a Gatan SC1000 ORIUS CCD camera with image size of 2048 × 2048 pixels. To identify interface structure at atomic resolution, HRTEM was carried out on cross-sectional TEM (XTEM) specimens in the same microscope. The point-to-point resolution of this microscope is 0.17 nm. Electron diffraction was used to identify the orientation relationships between Nb films and MgO substrates. HRTEM images were processed by using the image processing software of Gatan Digital Micrograph with fast Fourier transform (FFT) algorithm. Specimens with MgO(100) substrates were cut along the MgO(010) plane or MgO(001) plane and specimens with MgO(111) substrates were cut along the MgO($1\bar{1}0$) or MgO($11\bar{2}$) plane, which are all perpendicular to the interfaces, respectively, in order to observe interface structure easily at in-zone conditions in TEM. Samples were glued face to face with M-610 bond at room temperature. XTEM specimens were prepared by using a dimple grinder on a MultiPrep System followed by low energy ion milling with Ar ions at low angle on a Gatan PIPS System to reach electron transparent.

3. Results

3.1. General features of interface structure

Nb has a bcc structure with a lattice parameter of 0.3307 nm and MgO has a sodium chloride structure with a lattice parameter of 0.4217 nm. The binary phase

diagram of Nb and Mg indicates that they are completely immiscible over the full range of synthesis temperatures [32,33]. No ternary phase diagram exists for Nb, Mg and O. This implies that no interphase and no intermixing of Nb, Mg and O across the interface occur and thus the interfaces between Nb films and MgO substrates should be chemically abrupt at dimensions of several atomic layers, even for synthesis at the elevated temperature of 950 °C.

Fig. 1 shows XRD θ–2θ patterns of Nb films on MgO(100) (black line) and MgO(111) (gray line) substrates, respectively. Both films exhibit strong textures without any second phases. For Nb film on the MgO(100) substrate, only the strong reflection of Nb(100) is observed from the film, indicating that the film is strongly textured with the Nb(100) plane parallel to the MgO(100) plane. Diffraction peaks from other Nb orientations are absent. For Nb film on the MgO(111) substrate, only the diffraction peak of Nb(110) is present, together with diffraction peaks of MgO(111) and MgO(222) from the MgO(111) substrate. No extra diffraction peaks from other Nb orientations are observed. This confirms that the Nb film has a strong texture of the Nb(110) plane parallel to the MgO(111) substrate plane.

Fig. 2a shows a bright-field XTEM micrograph from Nb film on the MgO(100) substrate taken under an in-zone condition with the zone axis of MgO[001]. The difference in atomic number between Nb and MgO allows discriminating between the film and the substrate due to contrast differences in the lattice image. The atomic number of Nb is higher than the average atomic number of MgO, so the dark contrast in the image is identified as Nb. The Nb thin film thickness measured from the TEM image is ~180 nm, which is consistent with experimental expectation. The figure reveals that the Nb film exhibits a single-crystal-like

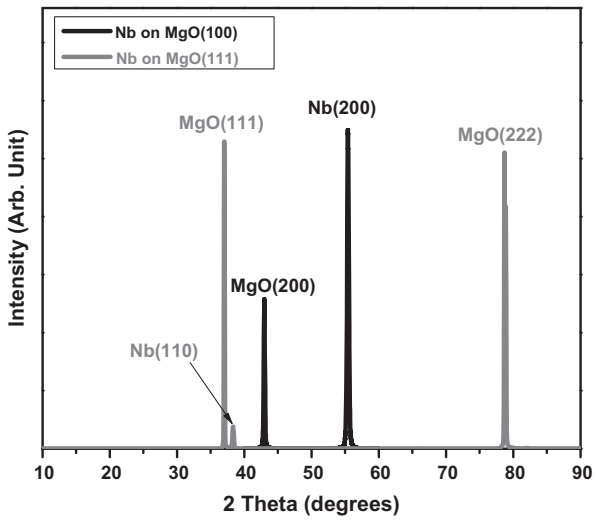

Fig. 1. XRD θ–2θ patterns of Nb film on MgO(100) (in black) and Nb film on MgO(111) (in gray) films deposited by e-beam evaporation. Results indicated that both films have strong textures without any second phases.

structure without grain boundaries. No porosities or cavities are observed in the thin film. The interface between Nb film and the MgO substrate is straight and clear without intermixing. The corresponding selected area diffraction (SAD) pattern is shown in Fig. 2b. The specimen was tilted prior to recording the SAD pattern so that the electron beam was parallel to the zone axis of MgO[001] in single crystal MgO(100). Meanwhile, the SAD pattern shows that the zone axis of Nb[011] is parallel to MgO[001], and the Nb(100) is parallel to MgO(100), e.g. Nb[011]//MgO[001] and Nb(100)//MgO(100), a well-defined orientation relationship between Nb film and the MgO(100) substrate. This orientation relationship is consistent with the XRD observation, e.g. Nb(100)// MgO(100). In the following, Nb film on single crystal MgO(100) will be written as Nb(100)/MgO(100)

For single crystal MgO(100), two major low-index directions perpendicular to each other are the [010] and [001] directions within the MgO(100) plane. The SAD pattern shows that Nb(100) is parallel to MgO(100) and Nb[011] is parallel to MgO[001]. This indicates that the Nb(100) plane is rotated by 45° around the Nb[100] axis to minimize the lattice mismatch between these two dissimilar materials during growth.

For single crystal MgO(111), two major low-index directions perpendicular to each other within the MgO(111) plane are MgO[$1\bar{1}0$] and MgO[[$11\bar{2}$]. As a result, the observations of interface structure in TEM images from different in-zone directions of MgO[$11\bar{2}$] and MgO[$1\bar{1}0$] could be different. Fig. 3a demonstrates the bright-field XTEM image of Nb thin film on the MgO(111) substrate observed along the in-zone direction of MgO[$11\bar{2}$]. The film thickness measured from the TEM image is ~180 nm, which is the same as for Nb(100)/MgO(100). This implies no influence of substrate orientation on the film thickness during sample growth. The image shows that the film has a dense structure without grain boundaries. But more defect features such as dislocations are observed in the figure compared to Nb(100)/ MgO(100), indicating a lower crystalline quality for the Nb film on the MgO(111) substrate. A flat interface without interdiffusion between thin film and substrate is revealed in the TEM image. The corresponding SAD pattern shown in Fig. 3b indicates the well-defined orientation relationship between Nb and MgO(111), which is Nb(110)//MgO(111) and Nb[$1\bar{1}0$]//MgO[$11\bar{2}$].

Fig. 3c illustrates the bright-field XTEM image of Nb film on MgO(111) taken under in-zone conditions. The in-zone axis is MgO[$1\bar{1}0$], as revealed by the corresponding SAD shown in Fig. 3d. The image exhibits similar features to those observed from the in-zone axis of MgO[$11\bar{2}$]. SAD shows the same crystallographic plane orientation relationship of Nb(110)//MgO(111) (this film will be written as Nb(110)/MgO(111) in the following) as the observations from the in-zone axis of MgO[$11\bar{2}$], also consistent with XRD observations of Fig. 1 (gray line). The difference is that the direction of Nb[001] is parallel to MgO[$1\bar{1}0$].

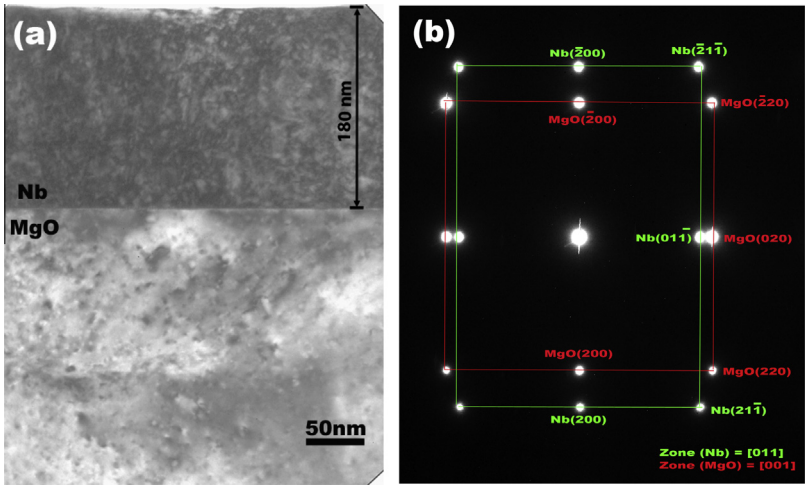

Fig. 2. (a) Bright-field XTEM micrograph of Nb(100)/MgO(100) (lattice mismatch between MgO(020) and Nb(011) is 10.3%). No columnar grain structure was observed in the film. (b) Corresponding selected area diffraction (SAD) pattern shows that the films exhibit the single-crystal-like structure and well-defined orientation relationship of interface.

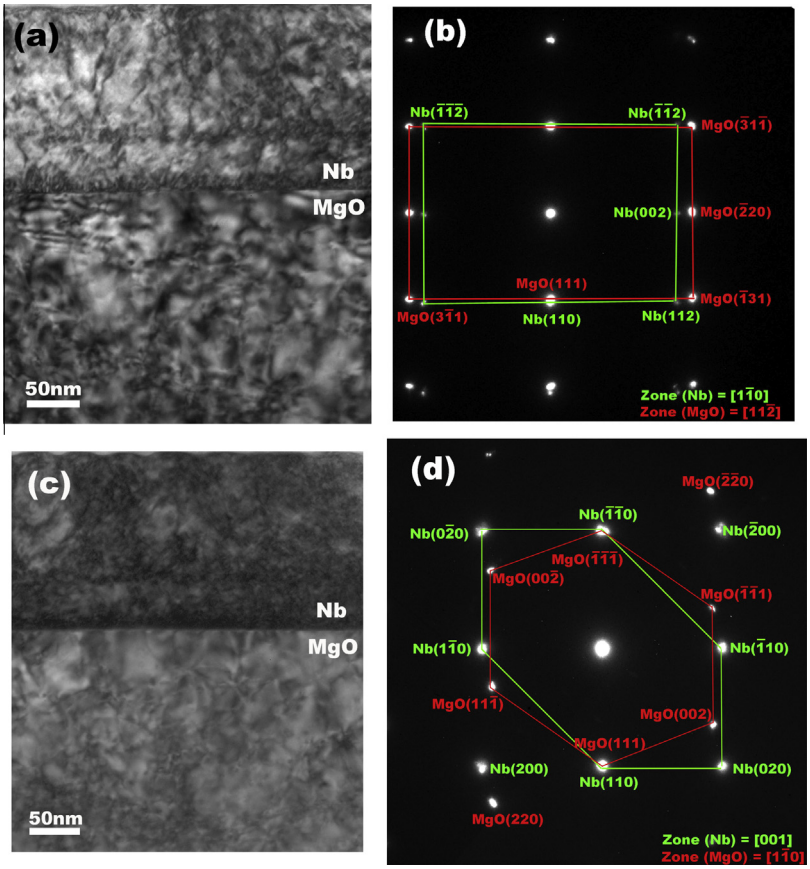

Fig. 3. (a) Bright-field XTEM micrograph of Nb(110)/MgO(111) observed along the zone of MgO[1 1 $\bar{2}$]. (b) Corresponding selected area diffraction (SAD) patterns. (c) Bright-field XTEM micrograph of Nb(110)/MgO(111) observed along the zone of MgO[1 $\bar{1}$ 0]. (d) Corresponding selected area diffraction (SAD) pattern. No columnar grain structure is observed in both films. Both SAD patterns indicate that the films exhibit the single-crystal-like structure and well-defined orientation relationship of interface.

Another difference is that the direction of Nb[1 $\bar{1}$ 0], perpendicular to the interface, has a tilt angle of 20°, with the direction of MgO[1 1 $\bar{1}$] across the interface. The horizontal lines at ~50 nm above the Nb/MgO interface plane in Fig. 3a and c were observed. These horizontal lines are composed of a higher density of the defects, which could be induced by the abnormity during thin film growth. Although XRD and SAD patterns reveal that Nb film

and the MgO substrate have different interface orientation relationships, which depend on the orientation of the single crystal substrate, the detailed atomic structure could not be resolved by XRD and TEM. Therefore, HRTEM was applied to characterize the atomic structure of the interface between Nb films and single crystal MgO substrates with different orientations.

3.2. Atomic structure of Nb(100)/MgO(100) interface

Understanding the atomic structure is essential and necessary to know how to tune and deploy the properties of materials with interface structure. Although XRD and TEM with SAD patterns reveal the orientation relationships of the interface between Nb films and MgO substrates, it is impossible to resolve the atomic structure of interfaces from these techniques. In order to fully understand the interface structure at atomic resolution, HRTEM studies were carried out.

Fig. 4a shows a HRTEM micrograph of Nb(100)/MgO(100) viewed along the MgO[001] zone axis, and also along Nb[011], as they are parallel to each other. The figure shows that the interface is atomically flat and sharp without any second phase over a large area. The absence of a second phase is attributed to full immiscibility between Nb and Mg. The periodic strain contrast visible along the interface is an indication of edge misfit dislocations. In order to clearly observe misfit dislocations, the region in Fig. 4a indicated by the box is enlarged and filtered by Fourier processing software through the diffraction spots of Nb(100) and MgO(100), as shown in Fig. 4b. The magnified figure shows that the interface is not absolutely straight, which could be due to the surface steps on the surface of MgO(100). Surface steps have been reported previously and attributed to internal oxidation of the Cu/MgO(100) interface [34]. The roughness of the interface shown in Fig. 4a is less than 1 nm (three atomic layers). The extra half atomic planes with periodic distribution, parallel to each other and almost normal to the interface, are clearly observed along the interface. This observation shows that the misfit dislocations can be viewed edge-on. Their cores are labeled $\top$ or $\perp$ in the figure. The dislocation cores are located at the interface and sit on the planes of Nb(01$\bar{1}$) and MgO(020) adjacent to the interface. Fig. 4c shows a Burgers vector of the dislocations determined by drawing a Burgers circuit around the misfit dislocation. The Burgers vector of the dislocation was determined as $b = 1/2$Nb[11$\bar{1}$]. Meanwhile, the tilting of the Nb film with respect to the substrate was observed in Fig. 4b. The tilting could be due to the existence of the dislocation with a Burgers vector of 1/2[11$\bar{1}$], which is not parallel to the interface. We speculate that this kind of dislocation is a result of the surface step on the surface of the MgO substrate. Previous studies reported that the single crystal MgO has the surface step [34]. Nb has a lattice parameter of 0.3307 nm and MgO has a lattice parameter of 0.4217 nm. If we assume that there is a surface step (one atomic layer) on the MgO surface, one interplanar spacing

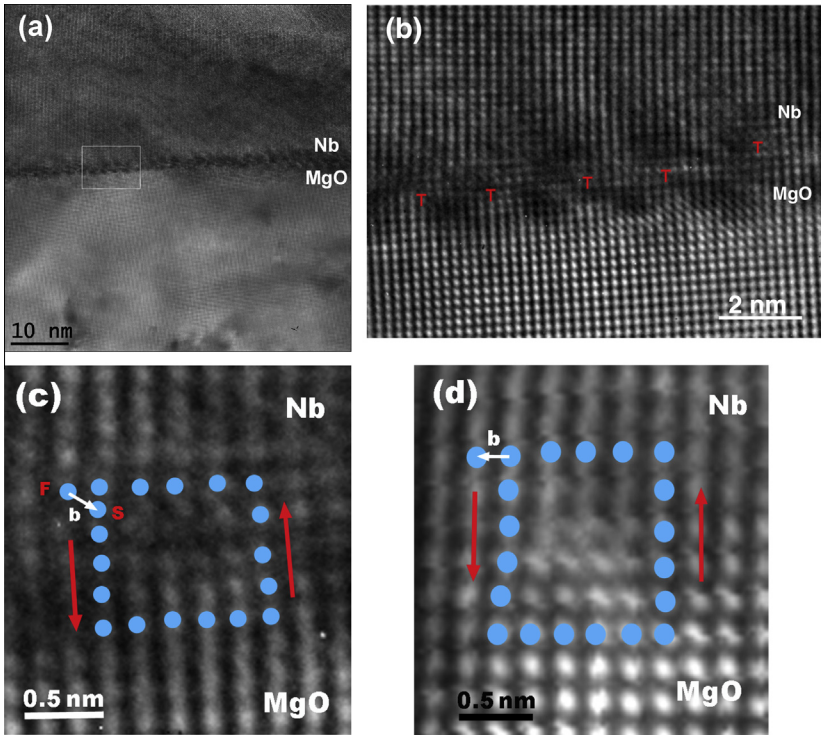

Fig. 4. (a) HRTEM micrograph of Nb(100)/MgO(100) observed along the zone of MgO[001]. (b) Enlarged image of the region labeled by the box in (a). (c) The drawing of the Burgers vector determined as ½Nb[11$\bar{1}$] by circuits around dislocation. (d) The drawing of the Burgers vector determined as ½Nb[01$\bar{1}$] by circuits around dislocation.

of Nb(200) atomic layer is smaller than the surface step and two interplanar spacings of Nb(200) are bigger than the surface step, so the mismatch between MgO(200) and Nb(200) in the region of surface step could induce the dislocation with a Burgers vector of ½[11$\bar{1}$]. As a result, the tilting of Nb film with respect to the substrate is created. On the other hand, we also observed another situation. Fig. 4d shows the drawing of the Burgers vector determined by plotting Burgers circuits around another dislocation. The Burgers vector of dislocation is determined as ½Nb[01$\bar{1}$]. No tilting of Nb film with respect to the substrate was observed. This could be due to the region where MgO(100) doesn't have surface step. Therefore, the dislocations along the interface between Nb film and MgO(100) substrates could have two types. The dislocation has a Burgers vector of ½[11$\bar{1}$], not parallel to the interface, which could be due to surface step on the surface of MgO(100). The dislocation has a Burgers vector of ½[01$\bar{1}$], parallel to the interface, which could be due to no surface step on the surface of MgO(100) and the value of the Burgers vector of ½[01$\bar{1}$] is 0.2338 nm. The average dislocation spacing between dislocations with a Burgers vector of ½[01$\bar{1}$] measured from the HRTEM image (not shown here) is 1.9 nm. If one assumes that the interface misfit dislocation is fully accommodated by the relaxation of the in-plane lattice mismatch, the interface dislocation spacing can be given by:

$$d = b/\delta \tag{1}$$

where b is the Burgers vector of the misfit dislocation and has a direction parallel to the interface, and δ, as lattice mismatch between film and substrate in this case, can be given by:

$$\delta = 2(d_{\mathrm{Nb}(011)} - d_{\mathrm{mgO}(020)})/(d_{\mathrm{Nb}(011)} + d_{\mathrm{MgO}(020)}) = 10.3\% \tag{2}$$

The calculated spacing between dislocations is $d = 0.2338/10.3\% = 2.3$ nm. This calculated value is larger than the measured value of 1.9 nm. Previous studies observed that the calculated dislocation spacing is 3–5% lower than measured because residual stress still exists after part of the mismatch strain is released by accommodating misfit dislocations [24]. In the current case, the observation that the calculated dislocation spacing is larger than the experimental one could be due to the fact that the distribution of misfit dislocations is non-uniform and the observed region has a higher density of misfit dislocations. Another possible reason is that the extra misfit dislocations could accommodate the intrinsic stress created during growth in the film.

3.3. Atomic structure of Nb(110)/MgO(111) interface

For Nb(110)/MgO(111), the interface structure is much more complicated than that in Nb(100)/MgO(100) as there are two different major low-index directions (e.g. MgO[11$\bar{2}$] and MgO[1$\bar{1}$0]) perpendicular to each other within the MgO(111) plane. As a result, the observations along these two directions exhibit different features of interface structure. In the film of Nb(100)/MgO(100), the observations along two directions perpendicular to each other are the same. Fig. 5a shows the HRTEM micrograph of the Nb(110)/MgO(111) interface structure viewed along MgO[11$\bar{2}$]. The image shows that the interface is atomically flat without diffusion. The interface roughness is less than 1 nm (three atomic layers). The SAD pattern in Fig. 3b shows Nb[002]//MgO[$\bar{2}$20], indicating that the lattice mismatch is $\delta = 2(d_{\mathrm{Nb}(200)} - d_{\mathrm{MgO}(220)})/(d_{\mathrm{Nb}(200)} + d_{\mathrm{MgO}(220)}) = 10.1\%$. The misfit dislocations should be viewed edge-on and located along the interfaces like those observed along the interface in the sample of Nb(100)/MgO(100). The d spacings of Nb(002) and MgO($\bar{2}$20) are 0.165 nm and 0.149 nm, respectively. The microscope resolution is 0.17 nm, thus these d spacing values are beyond the limit of this microscope resolution, so the structure of the dislocation cannot be directly resolved in this projection. However, since the interface structure and lattice mismatch for the film of Nb(110)/MgO(111) viewed along MgO[11$\bar{2}$] are very similar to those in Nb(100)/MgO(100) viewed along MgO[001], we speculate that the misfit dislocations will be located along interfaces periodically and sit on the planes of Nb(002) and MgO($\bar{2}$20). The extra half planes will be in the plane of MgO($\bar{2}$20) since the d spacing of

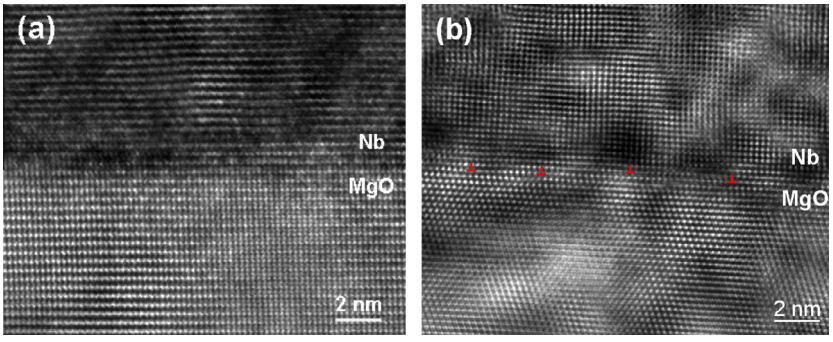

Fig. 5. (a) HRTEM micrograph of Nb(110)/MgO(111) observed along the zone of MgO[11$\bar{2}$]. (b) HRTEM image of Nb(110)/MgO(111) observed from the zone-axis of MgO[1$\bar{1}$0].

these planes is smaller than those of Nb(200). The projected Burgers vector will be $b = 1/2\mathrm{MgO}[\bar{1}10]$. So the calculated dislocation spacing is 1.5 nm, smaller than the one in the film of Nb(100)/MgO (100). Therefore, the density of the misfit dislocations along the interface in the film of Nb(110)/MgO(111) will be higher.

On the other hand, the cross-sectional HRTEM image of Nb(110)/MgO(111) observed from the MgO[$1\bar{1}0$] direction is shown in Fig. 5b. The image shows that the interface between film and substrate is sharp without intermixing and the interface roughness appears to be less than 1 nm. The misfit dislocations with the extra half planes perpendicular to the interface are observed on the Nb side. Their cores are labeled $\top$ and $\perp$ in the figure. The misfit dislocations exist due to the lattice mismatch between Nb($1\bar{1}0$) and MgO($11\bar{1}$) although they are not parallel to each other. The SAD pattern in Fig. 3d shows that Nb($1\bar{1}0$) is perpendicular to the interface and the MgO($11\bar{1}$) plane has a 20° rotation to the Nb($1\bar{1}0$). The MgO($11\bar{1}$) planes are discontinued when they cross the interface. No intermixing is observed by HRTEM. Due to the existence of a 20° rotation between Nb($1\bar{1}0$) and MgO($11\bar{1}$), the distance between MgO($11\bar{1}$) along the interface used for calculating lattice mismatch is determined in such a way that the d spacing of MgO($11\bar{1}$) is divided by cos20°, e.g. $d_{20} = d_{\mathrm{MgO}(111)}/\cos(20) = 0.2591$ nm. The lattice mismatch between Nb($1\bar{1}0$) and MgO($11\bar{1}$) with the rotation of 20° is $\delta = |2(d_{\mathrm{Nb}(110)} - d_{20})|/(d_{\mathrm{Nb}(110)} + d_{20}) = 10.2\%$. Thus the average spacing between misfit dislocations is $d = 0.2338/10.2\% = 2.3$ nm, where 0.2338 nm is the value of the projected Burgers vector in Nb film. The measured average spacing between dislocations is 3.5 nm, larger than the calculated value. This could be due to the existence of residual stress after part of the mismatch strain is released by accommodating misfit dislocations [24].

Van der Merwe [35–37] suggested that a thin film can grow on a rigid substrate such that the lattice mismatch between film and substrate is accommodated by elastic straining of the film before reaching critical thickness of h_c and by the introduction of misfit dislocation after exceeding the critical thickness. Critical thickness can be given by Matthews' equation below:

$$h_c = \frac{G_s b[\ln(h_c/b) + 1]}{4\pi(G_f + G_s)(1+\mu)\delta} \quad (3)$$

where G_s and G_f are shear moduli, μ is Poisson's ratio for the film, δ is the lattice mismatch and b is magnitude of the Burgers vector of the misfit dislocation; the subscripts s and f denote the substrate and the film, respectively. The value of critical thickness of Nb/MgO based on Matthews' equation is around a few nm, which is much smaller than the thickness of the Nb film, so misfit dislocations are induced to accommodate the lattice mismatch in all cases.

From the experimental results above, we clearly concluded that Nb(100) is the only plane preferred to grow on the single crystal MgO(100), and Nb(110) is the only plane preferred to grow on the single crystal MgO(111). However, it is not clear why the system chooses the interface as Nb(100)/MgO(100) and Nb(110)/MgO(111). In the following section, we attempt to understand these phenomena by means of first-principles calculations. Our sequent results show that, only when the system has the interface configuration of Nb(100)/MgO(100) and Nb(110)/MgO(111), the corresponding interfaces have the strongest interaction, which thus leads to a largest work of separation in the system. This criterion may shed light on the understanding of interfaces between different materials.

4. Discussions

4.1. Computational model and method to understand the interface structure from the first-principles calculations

In current first-principles studies, two complementary approaches are used for quantum mechanical modeling of interface: a small cluster of atoms and a periodic slab of crystal layers [38]. The cluster model is widely used to accurately provide the adsorption energy and bounding strength of adatoms or clusters deposited on oxide surfaces. The periodic slab model, which could be divided into coherent and incoherent periodic models, represents an interface as a sandwich of semi-infinite crystal layers and can take account of the metallic binding character; thus this model is extensively used to calculate the metal/oxide interfaces.

For the Nb/MgO system, our experiments show that the real Nb/MgO interface is incoherent, confirmed by a two-dimensional network of misfit dislocations. However, it is not plausible to use the incoherent interface models for the Nb/MgO system in first-principles calculations, because the lattice mismatch between Nb and MgO is relatively small, thus the corresponding Nb/MgO incoherent interface model must contain at least 1000 atoms, which are beyond the upper limit of this method. Fortunately, some researchers pointed out that properties of the incoherent interface could be approximated by weighted averages of properties of coherent interfaces that differ in their parallel translation [39,40]. Furthermore, Van der Merwe suggested that a thin film can grow coherently on a rigid substrate up to a critical thickness of h_c, after which it is energetically favorable for misfit dislocations to accommodate the lattice mismatch [35]. Even if the thickness of a thin film is larger than the critical thickness and interface misfit dislocations accommodate the lattice mismatch, the thin film initially grows coherently on the substrate at beginning. Thus it is still reasonable to use the coherent interface approximation to study the influence of lattice mismatch on the interface structure. The purpose of the simulation is to use the periodic slab model with the coherent interface approximation to verify and understand the experimental results of

interface structure and orientation relationships in the Nb films on MgO substrates.

For a given MgO plane, theoretically there could be an infinite number of Nb planes to match this MgO substrate. Experimental experiences with interface fabrication methods indicate the existence of "special" orientations between metal and oxide crystals. Often these special orientations are such that low-indexed planes and directions of one crystal lie parallel to low-indexed planes and directions in another crystal [3,31,41]. Therefore we only choose three lowest-indexed planes of Nb (Nb(100), Nb(110) and Nb(111)) to match the single crystal MgO (MgO(100) and MgO(111)) in current simulations, respectively.

The coherent Nb/MgO interface system is built by placing Nb layers on the top of MgO layers with slab geometry. For example, Fig. 6a shows the periodic slab model for Nb(100)/MgO(100) with a coherent interface. The process to build this model is as follows.

Firstly, we find out all the cells on a surface area (4×4 unit cell) for Nb(100) and MgO(100) and get all the possible cell match patterns for Nb(100)/MgO(100) with different cell shapes and orientations. Previous studies on bcc metal films deposited on MgO reported that bcc metal atoms usually sit on the top of either O or Mg atoms [31,41,42], so two types of coherent interface configurations were considered in the present calculations, where Nb atoms sit on the top of either O or Mg atoms, denoted as O-atop and Mg-atop, respectively. Secondly, we need to choose a match pattern between Nb and MgO at the interface for the following calculations. Early experimental and theoretical works show that the lattice misfit between thin film and substrate plays an important role in determining the atomic structure of the interface. Smaller lattice misfit leads to smaller misfit strain between the metal film and substrate [31,41,43]. The lattice misfit used here refers to the strain required to make a film coherent with a substrate, and is defined as:

$$\delta' = 1 - (2\Omega)/(S_1 + S_2) \tag{4}$$

where Ω represents the area of overlap of surface unit cells with the match cell area of S_1 in the thin film and the match area of S_2 in the substrate [40]. It is noted that δ' indicates the lattice misfit between to two planes, which differs from the lattice mismatch in one direction (δ). We therefore choose the match pattern in such a way that the lattice misfit is minimized to be the smallest. For example, in the Nb(100)/MgO(100) interface model, when the rectangle cell with the dimensions of 4.677×4.677 Å^2 on the Nb(100) plane matches the rectangle cell with the dimensions of 4.217×4.217 Å^2 on the MgO(100) plane, the misfit is minimized to be the smallest (10%). The corresponding orientation relationship between Nb and MgO in this case is Nb[011]//MgO[001] in the l direction, Nb[0$\bar{1}$1]//MgO[010] in the m direction and Nb[100]//MgO[100] in the n direction, as shown in Fig. 6a. Thirdly, we need to determine the changes in lattice constants for Nb due to the lattice misfit in the match pattern. We first stretch the length of the rectangle cell (in l and m directions

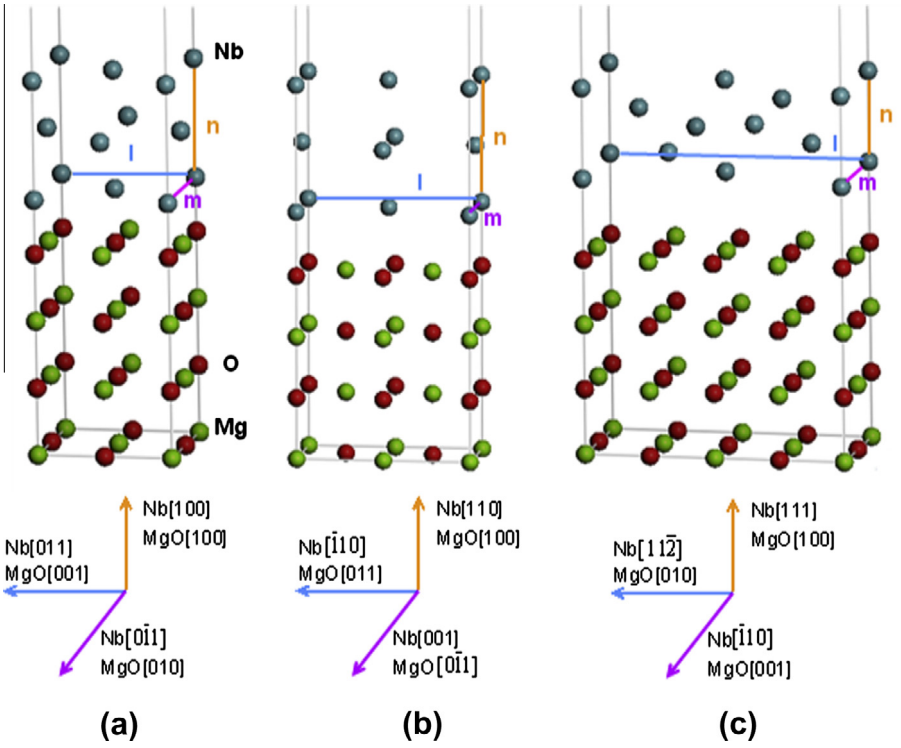

Fig. 6. Periodic slab model of three coherent Nb/MgO(100) interface models with the corresponding orientation relationships. (a) Nb(100)/MgO(100), (b) Nb(110)/MgO(100), (c) Nb(111)/MgO(100). l, m, n are the lattice constants for different orientations in the unit cell of stretched Nb.

of Fig. 6a) on the Nb(100) plane to match the cell on the MgO(100) plane with the dimensions of 4.217×4.217 Å^2, i.e., the deformation strain in l and m directions ([011] and [0$\bar{1}$1], respectively) for the Nb film is $\varepsilon_l = \varepsilon_m = (4.217 - 4.667)/4.667 = -10\%$. The shrinkage along the l and m directions of the Nb film leads to Nb lattice elongate along the n ([100]) direction. The lattice deformation along the n direction (ε_n) can be obtained by fixing $\varepsilon_l = \varepsilon_m = -10\%$ along the l and m directions and minimizing the total energy of the Nb film. For the present Nb(100)/MgO(100) system, $\varepsilon_n = (3.740 - 3.307)/3.307 = 13\%$, in which 3.740 Å is the new lattice distance along the n direction after minimization.

With all of the above information, we can build the periodic slab model for Nb(100)/MgO(100) with a coherent interface, as shown in Fig. 6a, in which it includes three layers of Nb(100), four layers of MgO(100) and a 1.5 nm vacuum slab. The interface distance x, defined as the nearest distance between the thin film atoms and substrate atoms, is a function of total energy of the whole interface system, and can be obtained by minimizing the total energy of the whole interface system with other parameters fixed. By repeating the above processes, we also obtained the periodic slab models for Nb(110)/MgO(100) (Fig. 6b), Nb(111)/MgO(100) (Fig. 6c), Nb(100)/MgO(111) (Fig. 7a), Nb(110)/MgO(111) (Fig. 7b) and Nb(111)/MgO(111) (Fig. 7c), respectively. In order to reduce the free surface effect in energy calculation, the number of Nb and MgO layers used in real calculation is six and eight, respectively.

With the established models, we can determine the interface configuration of the Nb/MgO system by analyzing the work of separation and electronic structure information of each model.

The work of separation is a fundamental quantity which characterizes the strength of the metal/ oxide interface. The work of separation W_{sep} is defined as the reversible work needed to separate the interface into two free surfaces. A larger work of separation often corresponds to a stable interface structure, and it can be written as [4]:

$$W_{\text{sep}} = (E_{\text{Nb}} + E_{\text{MgO}} - E_{\text{Nb/MgO}})/S \tag{5}$$

where W_{sep} is the work of separation and E_{Nb} is the energy of a single Nb slab, which is obtained by maintaining the parallel strains of the Nb slab. E_{MgO} is the energy of a single MgO slab; $E_{Nb/MgO}$ is the total energy of the whole interface. W_{sep} can be calculated either with free surface relaxation or without, allowing the free surface to relax. Here we use the later method, as Hashibon et al. [44] compared W_{sep} with different methods, and their results pointed out that the surface relaxation does not alter the hierarchy of the works of separation; therefore in order to determine the most stable structure it suffices to consider W_{sep} obtained without allowing the free surface to relax [44].

The structure optimizations and electronic structure calculations are performed by using the Cambridge Sequential Total Energy Package (CASTEP), which utilizes plane-wave pseudopotentials to perform first-principles quantum mechanics calculations [45]. The exchange-correlation

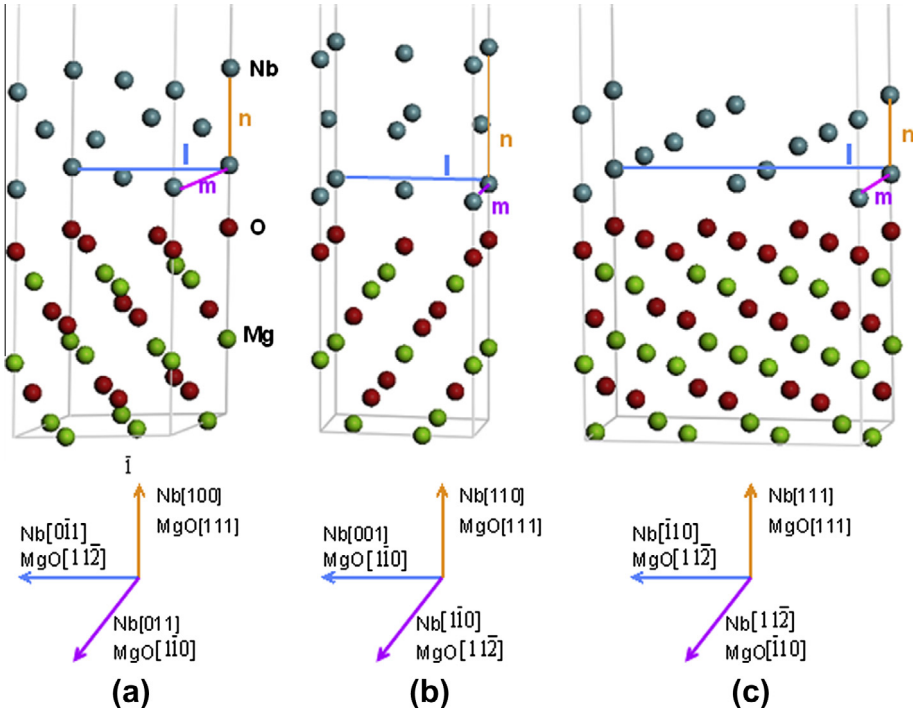

Fig. 7. Periodic slab model of three coherent Nb/MgO(111) interface models with the corresponding orientation relationships. (a) Nb(100)/MgO(111), (b) Nb(110)/MgO(111), (c) Nb(111)/MgO(111). l, m, n are the lattice constants for different orientations in the unit cell of stretched Nb.

potential is calculated by means of the generalized gradient approximation (GGA) using the Perdew–Wang 1991 (PW91) parameterization [46]. The plane wave basis set is limited by the cutoff energy of 340 eV, and the Brillouin zone is sampled by $8 \times 8 \times 1$ for most of the coherent interface models, which make the convergence tolerance energy 1.0×10^{-5} eV per atom, maximum force 0.03 eV Å^{-1} and maximum displacement 1.0×10^{-3} Å.

4.2. Understanding Nb(100) growth on single crystal MgO(100)

The calculated results of interface distance, for different coherent interface configurations presented in Fig. 6, are shown in Table 1. From this table we notice that, except for the Nb(111)/MgO(100) model, the interface distance of O-atop match type is smaller than that of the Mg-atop one, and the work of separation of O-atop match type is bigger than that of the Mg-atop match type. These results indicate that the Mg-atop match type is not preferred for the Nb(100)/MgO(100) system. To understand the reasons behind this phenomenon, we further calculate the difference in electron density for these two match types. Here electron density difference is calculated as follows:

$$\Delta\rho = \rho_{\mathrm{Nb/MgO}} - (\rho_{\mathrm{Nb}} + \rho_{\mathrm{MgO}}) \quad (6)$$

where $\rho_{\mathrm{Nb/MgO}}$ is the electron density of the Nb/Mgo interface structure and ρ_{Nb} and ρ_{MgO} are the electron densities of the Nb and MgO slabs having the same atomic positions in the interface structure. The O-atop and Mg-atop electron density difference results for Nb(100)/MgO(100) are shown in Fig. 8a and b. For the O-atop Nb(100)/MgO(100), there is a clear electron transfer from Nb atom to O atom, and electrons accumulation between the interface, as shown in Fig. 8a. The redistribution of electrons implies that the bonds along O-atop Nb(100)/MgO(100) have both covalent and ionic bond characteristics, similar to that occurring in the Ni/MgO or Cu/MgO interface structure [47]. In contrast, few electrons are localized between the interface for Mg-atop Nb(100)/MgO(100), as shown in Fig. 8b. This means that the interaction along the interface plane of O-atop match type is stronger than that in Mg-atop match type. As a result, the interface distance of O-atop is smaller than that in the Mg-atop match type, and the interface structure with O-atop match type is more stable. It is noted that the exception for the Nb(111)/MgO(100) model is due to the fact that both O-atop and Mg-atop match types have the same interface structure, and thus the same interface distance and work of separation.

For the three O-atop Nb/MgO(100) coherent interface models in Fig. 6, we note from Table 1 that the Nb(100)/MgO(100) model (shown in Fig. 6a) has the biggest work of separation, in contrast to the models with Nb(110)/MgO(100) and Nb(111)/MgO(100) (shown in Fig. 6b and c, respectively). This means that the O-atop Nb(100)/MgO(100) coherent interface structure is the most stable one among all the potential candidates (with low work of separation) that we have evaluated. It also indicates that Nb(100) is the only plane preferred to grow on the single crystal MgO(100). To further understand why Nb(100)/MgO(100) is preferred, we calculated the bond populations of all the three O-atop Nb/MgO(100) coherent interface models. Bond populations quantitatively describe the overlap of electrons between two atoms [48], therefore they provide chemical bond information along the interface. From the calculated nearest Nb–O bond populations for the O-atop match types (shown in Table 1), we can see that the bond population for Nb(100)/MgO(100) is 0.55e, which is larger than that in the other two models. This indicates that the Nb–O bond at the Nb(100)/MgO(100) interface is the strongest among the three models, and thus Nb(100)/MgO(100) is preferred.

Table 1
Structure parameters, works of separation and bond populations of Nb/MgO(100) coherent interface models.

Models	δ'	$(\varepsilon_1, \varepsilon_m, \varepsilon_n)$	Match type	x	W_{sep}	$P_{\mathrm{Nb–O}}$
Nb(100)/MgO(100) Nb[011]//MgO[001] Nb[0$\bar{1}$1]//MgO[010] Nb[100]//MgO[100]	0.10	(−10%, −10%, 13%)	O-atop Mg-atop	2.4 3.6	0.09 0.03	0.55
Nb(110)/MgO(100) Nb[$\bar{1}$10]//MgO[011] Nb[001]//MgO[0$\bar{1}$1] Nb[110]//MgO[100]	0.16	(28%, −10%, −6%)	O-atop Mg-atop	2.6 3.6	0.05 0.01	0.13
Nb(111)/MgO(100) Nb[11$\bar{2}$]//MgO[010] Nb[$\bar{1}$10]//MgO[001] Nb[111]//MgO[100]	0.07	(4%, −10%, 4%)	O-atop Mg-atop	2.8 2.8	0.02 0.02	0.34

δ' is the interface misfit between un-stretched Nb and MgO films; $(\varepsilon_l, \varepsilon_m, \varepsilon_n)$ is the deformation strain in l, m and n directions for Nb film; match type O-atop and Mg-atop means the Nb atom is located just above the O and Mg atom; x is the interface distance, given in Å. W_{sep} is the work of separation, given in eV Å^{-2}. $P_{\mathrm{Nb–O}}(e)$ is the bond population for the nearest Nb and O atoms.

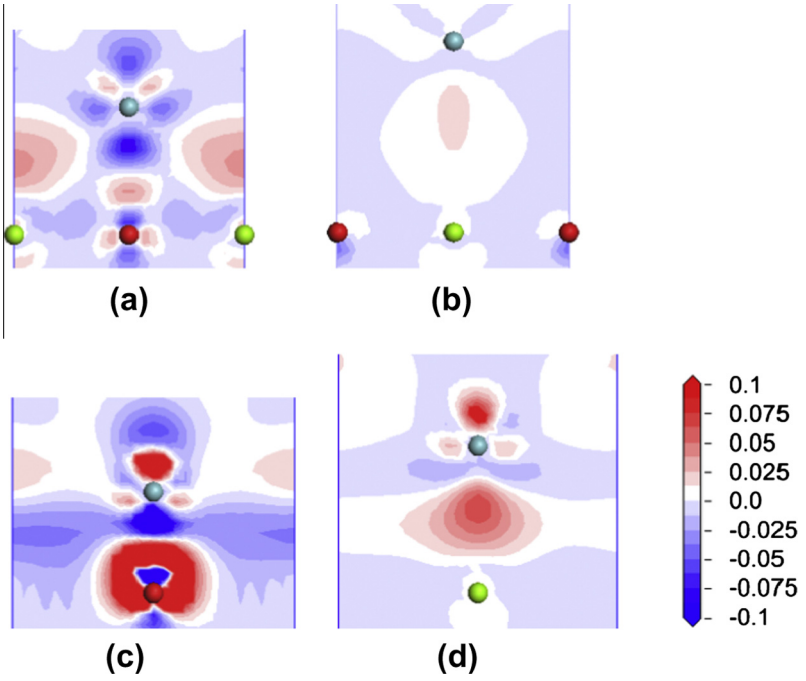

Fig. 8. Electron density difference maps for the coherent interface models along thte interfacial plane of Nb(100)/MgO(100) and Nb(110)/MgO(111); the positions of the interfacial atoms on interfacial cross section are indicated. (a) and (b) correspond to Nb(100)/MgO(100) with O-atop and Mg-atop match type; (c) and (d) correspond to Nb(110)/MgO(111) with O-atop and Mg-atop match type, respectively. The electron density difference are colored from −0.1 to 0.1 in the unit of electrons $Å^{-3}$.

4.3. Understanding Nb(110) growth on single crystal MgO(111)

Fig. 7 shows the periodic slab model of coherent interface configurations for Nb(100), Nb(110) and Nb(111) on single crystal MgO(111) substrates, respectively. Table 2 shows the structure parameters, interface distance and work of separation of these three Nb/MgO(111) coherent interface models. The table indicates that the interface structure of the O-atop match type is more stable than the Mg-atop match type. This is due to the fact that the interaction of Nb–O is stronger than Nb–Mg (shown in Fig. 8c and d) along the interface, which is the same as that observed for Nb(100)/MgO(100) coherent interface systems. For the O-atop Nb/MgO(111) coherent interface models, we further notice that the Nb(110)/MgO(111) model (Fig. 7b) with the orientation relationships of Nb[001]//MgO[1$\bar{1}$0], Nb[1$\bar{1}$0]//MgO[11$\bar{2}$] and Nb[110]//MgO[111], has the biggest work of separation among the three models. This implies that the Nb(110)/MgO(111) coherent interface structure is the most stable one among the three potential candidates. The reason for this is also that the nearest Nb–O bond for the O-atop Nb(100)/MgO(111) is the strongest. This results from the bigger

Table 2
Structure parameters, works of separation and bond populations of Nb/MgO(111) coherent interface models.

Models	δ'	(ε_1, ε_m, ε_n)	*Match type*	x	W_{sep}	P_{Nb-O}
Nb(100)/MgO(111)	0.15	(10%, 10%, −4%)	O-atop	2.0	0.40	0.96
Nb[0$\bar{1}$1]//MgO[11$\bar{2}$]			Mg-atop	2.1	0.10	
Nb[011]//MgO[1$\bar{1}$0]						
Nb[100]//MgO[111]						
Nb(110)/MgO(111)	0.10	(−10%, 10%, −1%)	O-atop	1.9	0.53	1.00
Nb[001]//MgO[1$\bar{1}$0]			Mg-atop	2.8	0.10	
Nb[1$\bar{1}$0]//MgO[11$\bar{2}$]						
Nb[110]//MgO[111]						
Nb(111)/MgO(111)	0.10	(10%, 10%, −12%)	O-atop	1.8	0.32	0.85
Nb[$\bar{1}$10]//MgO[11$\bar{2}$]			Mg-atop	2.5	0.10	
Nb[11$\bar{2}$]//MgO[$\bar{1}$10]						
Nb[111]//MgO[110]						

δ' is the interface misfit between unstretched Nb and MgO films; (ε_l, ε_m, ε_n) is the deformation strain in l, m and n directions for Nb film; match type O-atop and Mg-atop means the Nb atom is located just above the O and Mg atom; x is the interface distance, given in Å. W_{sep} is the work of separation, given in eV $Å^{-2}$. $P_{Nb-O}(e)$ is the bond populations for the nearest Nb and O atoms.

nearest Nb–O bond populations for Nb(110)/MgO(111) (1.00e) than that for Nb(100)/MgO(111) (0.96e) and Nb(111)/MgO(111) (0.85e).

We also calculated the difference in electron density for Nb(110)/MgO(111) interface with O-atop and Mg-atop match type, as shown in Fig. 8c and d. Similar to that in Nb(100)/MgO(100), we also find a clear electron transfer from Nb to oxygen atoms, whereas few electrons transfer between Nb and Mg atoms. This means that the interaction along the interface plane of O-atop Nb/MgO(111) is stronger than that in Mg-atop Nb/MgO(111). Comparing Fig. 8a with Fig. 8c, we can see that there are more electrons transferring from Nb to O in the Nb(110)/MgO(111) interface than that in the Nb(100)/MgO(100) interface, which means that the strength of the Nb–O ionic bond in the Nb(110)/MgO(111) interface is stronger than that in the Nb(100)/MgO(100) interface. This is also consistent with the high bond population and huge work of separation in the Nb/MgO(111) system (shown in Tables 1 and 2). The above phenomena may be closely related to the local atomic configuration along the interfacial plane to the interface system [47]. For O-atop MgO(111), the charge on the surface oxygen ion is not −2 units because MgO(111) is a non-stoichiometric plane. The oxygen ion can become −2 unit ions by charge transfer from Nb, providing a strong ionic bond along the Nb(110)/MgO(111) interface plane. In contrast, on MgO(100) the charge on the surface oxygen ion is already −2 units, since the MgO(100) is a stoichiometric plane. Hence the Nb–O ionic bond along Nb(100)/MgO(100) interface is weaker.

It is worth noting that we find that a Nb/MgO interface structure with the biggest work of separation does not always correspond to a Nb/MgO interface structure with the smallest misfit, as Nb(100)/MgO(100) and Nb(111)/MgO(100) show in Table 1. Higher separation energy means a more stable interface structure, and smaller misfit corresponds to more stable Nb films. However, the stability of the real interface system is related to both the stability of the Nb and MgO films and the stability of the interface structure. The present coherent interface models start from the models with minimum misfit, and the results show that the interface with the biggest work of separation is favored in experiments. This may indicate that although both misfit and work of separation are important for the interface structure metal/oxide system, the work of separation is the dominant factor that determines the orientation relationship between Nb thin films and single crystal MgO substrates.

5. Conclusion

Nb thin films were successfully deposited on single crystal MgO(100) and MgO(111) by electron beam evaporation, respectively. Well-defined orientation relationships of interfaces on both films have been confirmed experimentally, e.g. Nb(100)//MgO(100) and Nb[011]//MgO[001] for Nb films on MgO(100), and Nb(110)//MgO(111) and Nb[001]//MgO[$1\bar{1}0$] and Nb[$1\bar{1}0$]//MgO[[$11\bar{2}$] for Nb films on MgO(111). HRTEM revealed that the misfit dislocations are distributed along the Nb/MgO interfaces to accommodate the in-plane lattice mismatch between Nb film and MgO substrates. In Nb film on a MgO(100) substrate sample, we found two types of misfit dislocations. The misfit dislocation has a Burgers vector of ½Nb[$11\bar{1}$], which could be due to the step on the surface of MgO(100), and as a result, the tilting of Nb film with respect to the substrate was generated. The misfit dislocation has a Burgers vector of ½Nb[$01\bar{1}$] in the region where the surface of MgO(100) maybe doesn't have step, and no tilting of Nb films was created. First-principles calculations from a periodic slab model with a coherent interface approximation confirmed the experimental observations and showed that, only when the system has the interface configurations of Nb(100)/MgO(100) and Nb(110)/MgO(111), the corresponding interfaces have the strongest interactions, and this leads to the largest work of separation in the system. The work of separation is found to be the dominant factor that determines the orientation relationship between Nb thin films and single crystal MgO substrates.

Acknowledgements

The authors thank Dr. J.P. Hirth for insightful discussion, and thank Prof. Y.H. Chen for calculation assistance. This work was supported by the Center for Materials at Irradiation and Mechanical Extremes (CMIME), an Energy Frontier Research Center (EFRC) funded by the US Department of Energy, Office of Science, Office of Basic Energy Sciences under Award Number 2008LANL1026. The X-ray analysis portion of this work was supported by the Center for Integrated Nanotechnologies (CINT), a US Department of Energy, Office of Basic Energy Sciences user facility at Los Alamos National Laboratory (LANL). E.F. appreciates the support from The Recruitment Program of Global Youth Experts in China and the support of NSFC (11375018), and X.D. appreciates the support of NSFC (51171140, 51231008, 51320105014, and 51321003), the 973 Program of China (2010CB631003, 2012CB619402) and 111 project (B06025).

References

[1] Ruhle M, Evans AG, Ashby MF, Hirth JP, editors. Metal–ceramic interfaces. Oxford: Pergamon; 1990.
[2] Ruhle M. J Surf Anal 1997;3:157.
[3] Ernst F. Mater Sci Eng 1995;14:97.
[4] Finnis MW. J Phys: Condens Matter 1996;8:5811.
[5] Elshabini AAR, Barlow FD. The thin film technology handbook. New York: McGraw-Hill; 1997.
[6] Feniers F, Delplancke MP, Asskali A, Rooryck V, Van Sinay O. Appl Surf Sci 1996;92:35.
[7] Fu EG, Carter J, Swadener G, Misra A, Shao L, Wang H, et al. J Nucl Mater 2009;385:629.
[8] Fu EG, Misra A, Wang H, Shao L, Zhang X. J Nucl Mater 2010;407:178.

[9] Fu EG, Wang H, Carter J, Shao L, Wang YQ, Zhang X. Philos Mag 2013;93:883.
[10] Zhuo MJ, Fu EG, Yan L, Wang YQ, Zhang YY, Dickerson RM, et al. Scr Mater 2011;65:807.
[11] Zhang X, Fu EG, Misra A, Demkowicz MJ. JOM 2010;62:75.
[12] Zhuo MJ, Uberuaga BP, Yan L, Fu EG, Dickerson RM, Wang YQ, et al. J Nucl Mater 2012;429:177.
[13] Zhang X, Fu EG, Li N, Misra A, Wang YQ, Shao L, et al. J Eng Mater Technol 2012;134:041010.
[14] Han WZ, Demkowicz MJ, Fu EG, Wang H, Misra A. Acta Mater 2012;60:6341.
[15] Burger K, Mader W, Ruhle M. Ultramicroscopy 1987;22:1.
[16] Ernst F, Pirouz P, Heuer AH. Phil Mag A 1991;63:259.
[17] Mader W, Maier B. Colloque de Phys 1990;51:C1–867.
[18] Bialas H, Heneka K. Vacuum 1994;45:79.
[19] Hoel PH, Habermeier HU, Ruhle M. J Physique C 1985;4:141.
[20] Necker G, Mader W. Phil Mag Lett 1988;58:205.
[21] Florjancic M, Mader W, Ruhle M, Turwitt M. J Physique C 1985;4:141.
[22] Ernst P, Pirouz P, Heuer AH. Mater Res Soc Symp Proc 1989;138:557.
[23] Lu P, Cosandey F. Ultramicroscopy 1992;40:271.
[24] Lu P, Cosandey F. Acta Metall Mater 1992;40(Suppl.):S259.
[25] Grimmer H, Bollmann W, Warrington DH. Acta Crystallogr A 1974;30:197.
[26] Bollmann W. Crystal defects and crystalline interfaces. Berlin: Springer; 1970.
[27] Trampert A, Ernst F, Flynn CP, Fischmeister HF, Ruhle M. Acta Metall Mater 1992;40(Suppl.):S227.
[28] Zhukovskii YF, Kotomin EA, Jacobs PWM, Stoneham AM, Harding JH. Surf Sci 1999;441:373.
[29] Chen FR, Chiou SK, Chang L, Hong CS. Ultramicroscopy 1994;54:179.
[30] Ikuhara Y, Pirouz P, Yadavalli S, Flynn CP. Philos Mag A 1995;72:179.
[31] Ikuhara Y, Sugawara Y, Tanaka I, Pirouz P. Interface Sci 1997;5:5.
[32] ASM Alloy Phase Diagrams Center. <http://www.asminternational.org/AsmEnterprise/APD>.
[33] Smith JF. In: Massalski TB, editor. Binary alloy phase diagrams, vol. 3. 2nd ed. Materials Park, OH: ASM International; 1990. p. 2526.
[34] Backhaus-Ricoult M, Samet L, Trichet M-F, Hytch MJ, Imhoff D. J Solid State Chem 2003;173:172.
[35] Van der Merwe JH. Proc Phys Soc A 1950;63:616.
[36] Van der Merwe JH. Phil Mag 1962;7:1433.
[37] Van der Merwe JH. J Appl Phys 1963;34:117.
[38] Hong T, Smith JR, Srolovitz DJ. Acta Metall Mater 1995;43:2721.
[39] Benedek R, Seidman DN, Minkoff M, Yang LH, Alavi A. Phys Rev B 1999;60:16094.
[40] Benedek R, Seidman DN, Woodward C. J Phys: Condens Matter 2002;14:2877.
[41] Wang CM, Kaspar TC, Shutthanandan V, Joly AG, Kurtz RJ. Acta Mater 2011;59:4274.
[42] Matsunaga K, Sasaki T, Shibata N, Mizoguchi T, Yamamoto T, Ikuhara Y. Phys Rev B 2006;74:125423.
[43] Benedek R, Alavi A, Seidman DN, Yang LH, Muller DA, Woodward C. Phys Rev Lett 2000;84:3362.
[44] Hashibon A, Elsässer C, Rühle M. Acta Mater 2005;53:5323.
[45] Segall MD, Lindan PJD, Probert MJ, Pickard CJ, Hasnip PJ, Clark SJ, et al. J Phys: Condens Matter 2002;14:2717.
[46] Perdew JP, Wang Y. Phys Rev B 1992;45:13244.
[47] Matsunaka D, Shibutani Y. Phys Rev B 2008;77:165435.
[48] Heifets E, Zhukovskii YF, Kotomin EA, Causa M. Chem Phys Lett 1998;283:395.